18. C. Weitkamp, *Lidar: Range-Resolved Optical Remote Sensing of the Atmosphere* (Springer, New York, 2014).
19. E. Myslivets, B. P.-P. Kuo, N. Alic, S. Radic, *Opt. Express* **20**, 3331–3344 (2012).
20. V. Ataie, E. Myslivets, B. P.-P. Kuo, N. Alic, S. Radic, *J. Lightwave Technol.* **32**, 840–846 (2014).
21. Material and methods are available as supplementary materials on *Science* Online.
22. G. Jacobsen, *Noise in Digital Optical Transmission Systems* (Artech House, Boston, 1994).

ACKNOWLEDGMENTS

This work is funded in part by the Defense Advanced Research Projects Agency. University of California has filed a patent on the method and applications of random signal detection and coherent analysis.

SUPPLEMENTARY MATERIALS

www.sciencemag.org/content/350/6266/1343/suppl/DC1
Materials and Methods
Figs. S1 to S7
References (*23*–*29*)

20 August 2015; accepted 12 October 2015
10.1126/science.aac8446

SURFACE SCIENCE

Electron-hole pair excitation determines the mechanism of hydrogen atom adsorption

Oliver Bünermann,[1,2,3]* Hongyan Jiang,[1] Yvonne Dorenkamp,[1] Alexander Kandratsenka,[1,2] Svenja M. Janke,[1,2] Daniel J. Auerbach,[1,2] Alec M. Wodtke[1,2,3]

How much translational energy atoms and molecules lose in collisions at surfaces determines whether they adsorb or scatter. The fact that hydrogen (H) atoms stick to metal surfaces poses a basic question. Momentum and energy conservation demands that the light H atom cannot efficiently transfer its energy to the heavier atoms of the solid in a binary collision. How then do H atoms efficiently stick to metal surfaces? We show through experiments that H-atom collisions at an insulating surface (an adsorbed xenon layer on a gold single-crystal surface) are indeed nearly elastic, following the predictions of energy and momentum conservation. In contrast, H-atom collisions with the bare gold surface exhibit a large loss of translational energy that can be reproduced by an atomic-level simulation describing electron-hole pair excitation.

Adsorption of atomic hydrogen (H) is the simplest reaction in surface chemistry. Langmuir's study of this reaction ushered in the era of modern surface science (*1*). Hydrogen adsorption is important for many fields, ranging from heterogeneous catalysis (*2*) to interstellar molecular hydrogen production (*3*). Adsorbed H atoms can stabilize surfaces of intrinsically reactive solids, healing dangling bonds and making them suitable for industrial processing (*4*). Adsorption is also central to hydrogen storage technologies (*5*), and it is the basis for a chemical means of manipulating the band gap in graphene (*6*).

Despite more than a century of study, we still do not have a fundamental understanding of how H-atom adsorption takes place. Adsorption involves the H atom coming to rest at the surface, losing its initial translational energy, and dissipating the energy of the chemical bond formed with the solid (Fig. 1A). Because of its light mass, energy and momentum conservation requires that the transfer of H-atom translational energy to heavy surface atoms is inefficient; for example, an H atom colliding with a gold atom at a Au(111) surface is expected to transfer only 2% of its translational energy per collision (Fig. 1B). How then can the H atom lose sufficient translational energy to adsorb? As early as 1979, speculations were made, supported by theoretical analysis, that the mechanism of H-atom adsorption at metals could involve the conversion of H-atom translational energy to electronic excitation of the solid (*7*). This requires a failure of the Born-Oppenheimer approximation (BOA), which assumes that electronic motions are much faster than nuclear motions and can be treated separately (*8*). Although failure of the BOA is not without precedence—for example, infrared linewidths of chemisorbed H atoms on metals are believed to be broadened by electronic interactions (*9*), and "chemicurrents" have been detected at Schottky diode junctions (*10*–*12*)—there are no experimental measurements of the translational inelasticity of H atoms with any solid. Moreover, translational excitation of electron-hole pairs occurring because of collisions of atoms or molecules with surfaces has never been observed in the absence of efficient phonon excitation (*13*).

Previous experiments on BOA failure showed that highly vibrationally excited molecules exhibit efficient vibrational relaxation when they collide with a clean single-crystal metal surface, whereas little relaxation is seen with insulators (*14*, *15*). This comparison showed the importance of electronic excitation by molecular vibration, a phenomenon that could also be investigated with first-principles theory (*16*, *17*). Although vibrational relaxation studies tell us nothing about adsorption, they suggest an approach to the problem. If BOA failure were important in H-atom adsorption, we would expect inelastic H-atom scattering from metals and insulators to exhibit dramatic differences in their translational energy loss; furthermore, we could only describe the inelasticity with modern theoretical methods that account for electronic excitation (*18*–*20*).

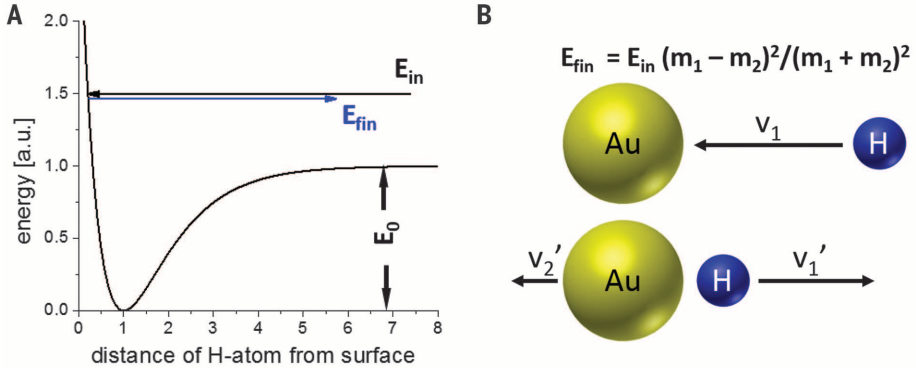

Fig. 1. Adsorption of H atom requires loss of translational energy. (**A**) The incident H atom must lose its initial translational energy, E_{in}, and dissipate the chemical potential energy, E_0, that it discovers in binding to the surface. (**B**) Conserving linear momentum and translational energy in a simple collinear binary collision model leads to a simple relation between E_{in} and the final kinetic energy of the H atom, E_{fin}, that depends only on the masses of the atoms. For the example of H ($m_1 = 1$) colliding with Au ($m_2 = 198$), the H atom retains 98% of its initial energy.

[1]Institute for Physical Chemistry, Georg-August University of Göttingen, Tammannstrasse 6, 37077 Göttingen, Germany. [2]Department of Dynamics at Surfaces, Max Planck Institute for Biophysical Chemistry, Am Faßberg 11, 37077 Göttingen, Germany. [3]International Center for Advanced Studies of Energy Conversion, Georg-August University of Göttingen, Tammannstrasse 6, 37077 Göttingen, Germany.
***Corresponding author. E-mail: oliver.buenermann@chemie.uni-goettingen.de**

Experiments probing inelastic H-atom scattering from surfaces are extremely challenging. Previous studies on H-atom scattering from solids used discharge-based H-atom sources and, in some cases, electromagnetic velocity filters (*21*, *22*). These approaches yield relatively broad H-atom velocity distributions that peak at low translational energies. Detecting H atoms is also challenging: Bolometers (*22*), photographic plates (*23*), and ZnO conductivity detectors (*24*) were sensitive enough to observe surface scattering, but their slow temporal response precludes the study of inelastic scattering. These experimental limitations help explain why, since the first successful observations of H atom scattering from surfaces (*23*), additional studies have measured spatially resolved diffraction rather than inelastic scattering.

Here, we show that the translational energy loss of H atoms colliding at a metal surface predominantly results from electronic excitation of the solid. We produced nearly monoenergetic incident beams of H atoms by laser photolysis, the energy of which can be varied (*25*, *26*), and obtained scattering-angle resolved, translational energy loss spectra by the Rydberg-atom neutral time-of-flight (TOF) method (*27*). Our measurements show that collisions of H atoms at metal surfaces are strongly inelastic. In contrast, H-atom collisions at an insulator are nearly elastic. For the insulator, the small inelasticity can be understood as a simple binary collision between a light and heavy atom where linear momentum is conserved. For H-atom energy loss at a metal, we used a recently developed full-dimensional molecular dynamics (MD) method (*20*) capable of describing both excitation of the solid lattice and electron-hole pairs. This model gives good agreement with experimental results. Switching off electron-hole pair excitation in the simulations resulted in energy loss far less than observed.

A schematic diagram of our apparatus (Fig. 2) shows the pulsed molecular beam expansion that efficiently cooled HI to its ground state, where ultraviolet (UV) laser photolysis produced nearly mono-energetic H atoms. A small fraction of these atoms passed through two differential pumping chambers (not shown), entered an ultrahigh vacuum (UHV) chamber, and collided with a gold (Au) single crystal. The incidence angles, ϑ_i and φ_i, were varied by tilting the Au crystal, which was held in a six-axis UHV manipulator. Recoiling H atoms were subjected to Rydberg tagging (*27*); that is, they were excited by two laser pulses to the long-lived n = 34 Rydberg state, which lies just ~10 meV below the ionization level. These neutral atoms passed a detector aperture and traveled 25 cm in a field-free region, and then through a grounded wire mesh, to encounter a weak (~7 kV/cm) ionizing field just in front of an ion counting detector. H-atom TOFs were recorded by a multichannel scalar. The detector could be rotated so that TOF data could be obtained at many scattering angles, ϑ_s.

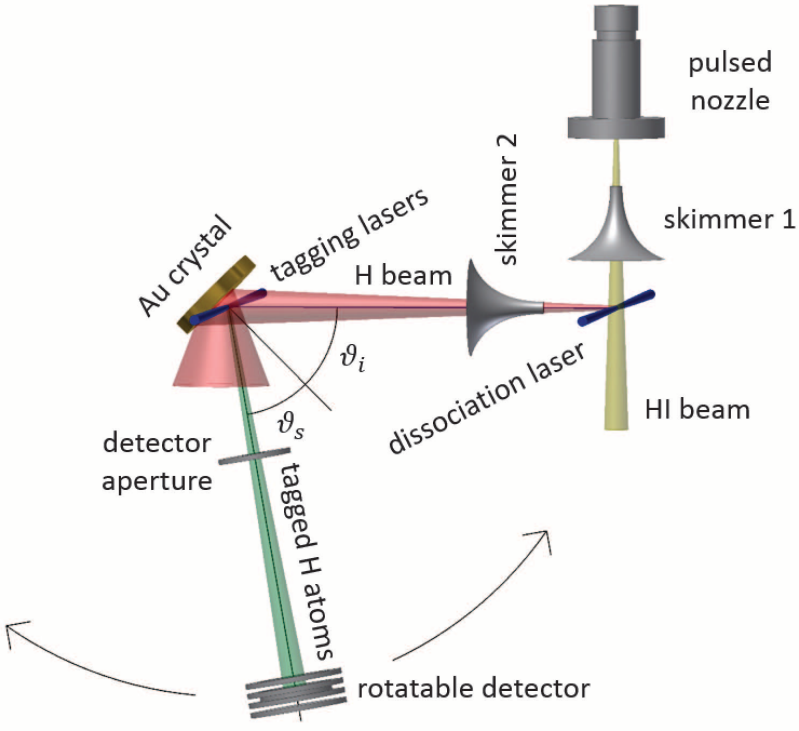

Fig. 2. Schematic of the experimental apparatus. A molecular beam of rotationally cold HI is formed in a pulsed molecular beam expansion. After skimmer 1, the HI beam is crossed by the dissociation laser beam. A small fraction of the H-atom photoproducts pass skimmer 2, pass through two differential pumping stages (not shown), and enter a UHV chamber. Here, they hit the surface of a Au single crystal held on a six-axis manipulator that allows the variation of the polar (ϑ_i) and azimuthal (φ_i) incidence angles. Scattered H atoms are tagged in a two-step process: first, a 121.57-nm photon brings the H atoms into the 2p state. Second, a 365.90-nm photon transfers the atoms into the n = 34 Rydberg state. A fraction of the tagged H atoms pass the detector aperture and travel 25 cm before they reach the detector, where their time of arrival is recorded. The detector is rotatable, allowing the variation of the scattering angle ϑ_s.

The Au surface was cleaned by cycles of Ar-ion sputtering and annealing at 1000 K. Auger electron spectroscopy (AES) and low-energy electron diffraction (LEED) were used to determine the cleanliness and orientation of the Au(111) surface. The Au sample could also be cooled to 45 K with cold gaseous He, allowing Xe condensation. We used a 300-Langmuir exposure (10^{-6} mbar Xe gas for 5 min) to produce a thick Xe layer (an insulating surface) whose structure was not influenced by the underlying Au crystal. Warming easily removed the Xe layer, allowing H-atom scattering measurements from metal and insulator to be made within minutes of one another.

Figure 3A shows representative TOF data for H-atom scattering from Au (open squares) and solid Xe (filled squares). The scattering conditions were E_{in} = 2.76 eV, $\vartheta_i = 45°$, $\vartheta_s = 45°$, and $\varphi_i = 0°$ with respect to the $[10\,\bar{1}]$ direction. Figure 3B shows the translational energy loss distributions derived from the TOF data using the appropriate Jacobian. The inset shows the measured translational energy distribution of the incident H atoms.

There is a stunning difference in the observed H-atom inelasticity for scattering from metallic Au and an insulating Xe layer. The most probable energy loss for H-atom scattering from solid Xe was 46 meV, somewhat lower than that expected for a collinear binary elastic collision between a H and a single Xe atom (83 meV, shown as a vertical arrow in Fig. 3). For H-atom scattering from gold, the average energy loss was 20 times as high (910 meV). This energy loss is far too large to be compatible with the expectation for a H/Au binary collision model (56 meV), yet it is still far too small to be the result of H-atom trapping followed by thermal desorption. Furthermore, in contrast to the H/Xe scattering, which shows a very specific energy loss, the energy loss distribution for H scattering from Au was remarkably broad, extending out to at least 2.0 eV, suggesting that a broad continuum of acceptor states in the solid contributes to the translational inelasticity. These remarkable observations are compelling evidence that H-atom translational energy is efficiently converted to electronic excitation in collisions with solid gold.

Although a binary electronically adiabatic collision model is sufficient to understand the essence of the H-atom scattering from solid Xe, more involved theory is needed to treat H-atom scattering from a metal (*18*, *19*). Accurately describing metal atom motion and electron-hole pair excitation are the two key challenges. Recently, we have developed an approach to MD simulations that self-consistently treats mechanical energy transfer to Au lattice motion

and electronic excitation (*20*). The MD is carried out on a global full-dimensional potential energy surface (PES) based on effective medium theory (EMT) fitted to ab initio electronic energies. Because the EMT intrinsically contains the embedded electron densities, we can self-consistently describe electronically nonadiabatic behavior on the level of the local-density electronic friction approximation (LDFA) (*28*), with no adjustable parameters. We performed MD calculations for several million trajectories, enough to make comparisons with the measurements of angle-resolved inelastic scattering.

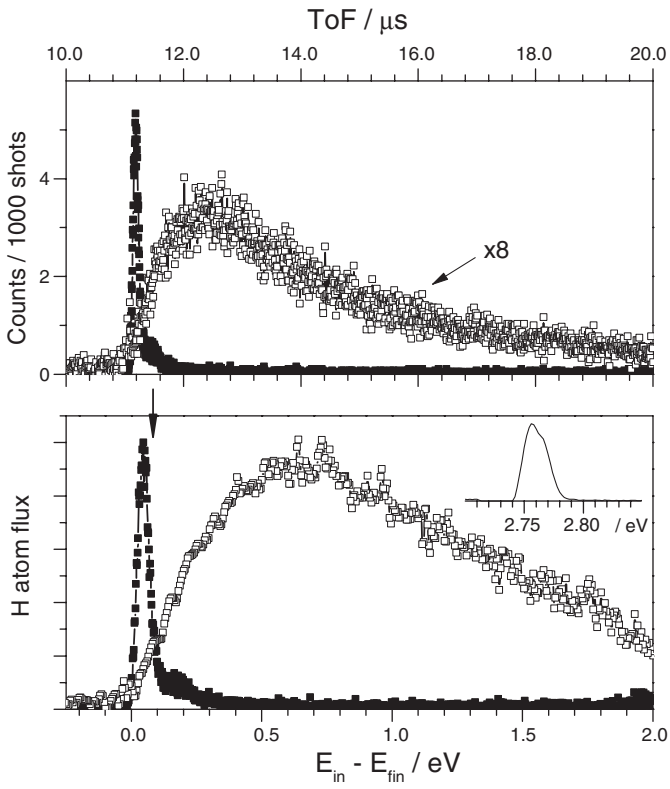

Fig. 3. Translational inelasticity for H-atom collisions with an insulator and a metal. (**Top**) Measured TOF spectra for H atoms scattered from Au(111) (open squares) and solid Xe (filled squares). The channel width is 8 ns for Au and 4 ns for Xe. (**Bottom**) Corresponding kinetic energy loss spectra obtained by Jacobian transformation of the TOF data. The inset shows the kinetic energy distribution of the incident H-atom beam. The vertical arrow marks the expected energy loss for a binary collision between an H and a Xe atom. The experimental conditions are E_{in} = 2.76 eV, ϑ_i = 45°, ϑ_s = 45° and ϕ_i = 0°, with respect to the [10$\bar{1}$] direction.

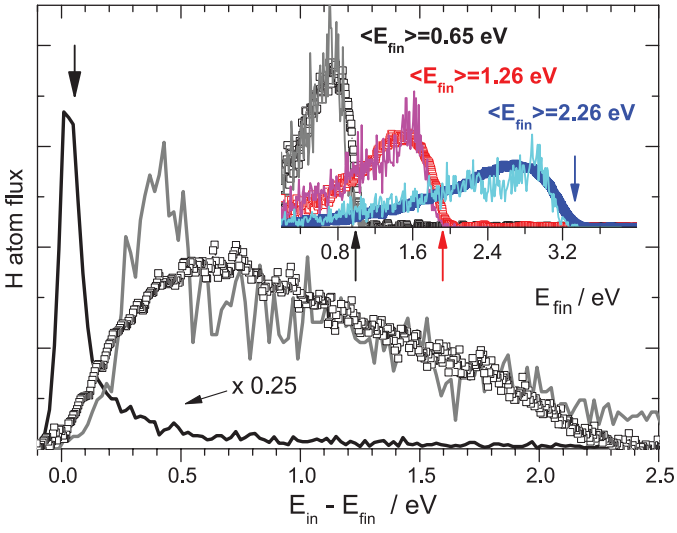

Fig. 4. Comparison of the experimentally obtained kinetic energy loss spectrum to theoretical simulations. Theoretical energy loss found when neglecting (solid black line) and including (solid gray line) electronic excitation. Experimental energy loss for E_{in} = 2.76 eV are shown as open squares. The vertical arrow marks the expected energy loss for a binary collision between an H and an Au atom. The inset shows the incidence energy dependence, E_{in}, of the experimentally derived translational inelasticity (open squares) and comparison to theory (solid lines): E_{in} = 3.33 eV (blue), 1.92 eV (red), and 0.99 eV (black). Colored arrows mark the three incidence energies. Also shown are the average final translational energies, $\langle E_{fin} \rangle$. The scattering angles are ϑ_i = 45°, ϑ_s = 45°, and φ_i = 0° with respect to the [10$\bar{1}$] direction. In all cases, the scattered H atoms remain unthermalized with the solid, emerging with a substantial fraction of their incidence translational energy.

Figure 4 shows some of these comparisons for H-atom scattering from Au(111). The solid black line shows the theoretical prediction, neglecting electronic excitation. The narrow energy loss distribution, peaking near the expected value for a binary collision of H with Au (56 meV, shown as a vertical arrow), clearly fails to capture the observed magnitude of the H-atom translational energy loss. The gray solid line shows the simulated energy loss distribution when electronic excitation is included in the MD simulations at the level of the LDFA. Here, the theoretical energy loss distribution captures the experimental result remarkably well. We have made extensive comparisons between experiment and theory, like those shown in Fig. 4 for a range of scattering angles, ϑ_i, φ_i, and ϑ_s; the agreement is uniformly good.

The inset to Fig. 4 shows how the translational inelasticity depends on the incidence energy and compares to electronically nonadiabatic MD simulations. At all incidence energies, agreement between experiment and theory is good and the energy loss is dominated by electronic excitation. We note that the fractional energy loss, $(E_{in} - \langle E_{fin} \rangle)/E_{in}$ = 0.33 ± 0.01, is nearly independent of E_{in}, meaning that electron-hole pair excitation remains important even at reduced incidence energies. This theoretical modeling confirms the qualitative statement made above: H-atom translational energy is efficiently converted to electronic excitation in collisions with solid gold.

The good agreement between experiment and theory is evidence for the validity of the approximations made in the MD simulations. Furthermore, the ability of the simulations to reproduce these experiments lends weight to the predictions made in (*20*). Most interesting among these are the predictions that electron-hole pair excitation increases the sticking probability and determines the adsorption mechanism, which occurs by penetration resurfacing. Here, H-atom adsorption occurs by initial population of subsurface binding sites (where electronic excitation is most efficient) followed by migration to the strongest binding sites, which are at the surface. This work also invalidates a previous alternative hypothesis, one where multiple electronically adiabatic collisions resulting from a conversion of normal to parallel H-atom momentum lead to sticking (*29*). Inspection of individual trajectories shows that such adsorption behavior occurs only when electronic excitation is included in the simulations (*20*).

This study demonstrates the importance of electronic excitation in atomic scattering at metal surfaces and provides a valuable benchmark for first-principles theories of energy transfer and adsorption. The prospect of using an experimentally validated electronically nonadiabatic theory of H interactions at a solid metal is exciting and could lead to progress on important problems, including H-atom diffusion in bulk metals and on metal surfaces, adsorbate influences on surface reconstruction, quantum dynamics of adsorption, and energetic atom diffusion and surface

penetration. More generally, chemical reactions at a metal surface are nearly always modeled within the adiabatic Born-Oppenheimer approximation; see, for example, (*30*). Our work suggests that theories of surface chemistry capable of describing electron excitation may be crucial to understanding atomic-scale motion occurring in surface reactions, especially if H-atom translation is involved.

REFERENCES AND NOTES

1. I. Langmuir, *J. Am. Chem. Soc.* **34**, 1310–1325 (1912).
2. M. P. Andersson *et al.*, *J. Catal.* **255**, 6–19 (2008).
3. D. Hollenbach, E. E. Salpeter, *Astrophys. J.* **163**, 155 (1971).
4. G. S. Higashi, Y. J. Chabal, G. W. Trucks, K. Raghavachari, *Appl. Phys. Lett.* **56**, 656–658 (1990).
5. S. M. Lee *et al.*, *Synth. Met.* **113**, 209–216 (2000).
6. D. Haberer *et al.*, *Nano Lett.* **10**, 3360–3366 (2010).
7. J. K. Norskov, B. I. Lundqvist, *Surf. Sci.* **89**, 251–261 (1979).
8. M. Born, R. Oppenheimer, *Annalen Der Physik* **84**, 457–484 (1927).
9. C. L. A. Lamont, B. N. J. Persson, G. P. Williams, *Chem. Phys. Lett.* **243**, 429–434 (1995).
10. H. Nienhaus *et al.*, *Phys. Rev. Lett.* **82**, 446–449 (1999).
11. B. Gergen, H. Nienhaus, W. H. Weinberg, E. W. McFarland, *Science* **294**, 2521–2523 (2001).
12. D. M. Bird, M. S. Mizielinski, M. Lindenblatt, E. Pehlke, *Surf. Sci.* **602**, 1212–1216 (2008).
13. A. Amirav, M.J. Cardillo, *Phys. Rev. Lett.* **57**, 2299 (1986).
14. Y. Huang, C. T. Rettner, D. J. Auerbach, A. M. Wodtke, *Science* **290**, 111–114 (2000).
15. K. Golibrzuch, N. Bartels, D. J. Auerbach, A. M. Wodtke, *Annu. Rev. Phys. Chem.* **66**, 399–425 (2015).
16. N. Shenvi, S. Roy, J. C. Tully, *Science* **326**, 829–832 (2009).
17. R. Cooper *et al.*, *Angew. Chem. Int. Ed.* **51**, 4954–4958 (2012).
18. M. Pavanello *et al.*, *Journal of Physical Chemistry Letters* **4**, 3735–3740 (2013).
19. G. J. Kroes, M. Pavanello, M. Blanco-Rey, M. Alducin, D. J. Auerbach, *J. Chem. Phys.* **141**, 054705 (2014).
20. S. M. Janke, D. J. Auerbach, A. M. Wodtke, A. Kandratsenka, *J. Chem. Phys.* **143**, 124708 (2015).
21. H. U. Finzel *et al.*, *Surf. Sci.* **49**, 577–605 (1975).
22. G. Caracciolo, S. Iannotta, G. Scoles, U. Valbusa, *J. Chem. Phys.* **72**, 4491–4499 (1980).
23. T. H. Johnson, *Phys. Rev.* **37**, 847–861 (1931).
24. K. Haberrecker *et al.*, *Nucl. Instrum. Methods* **57**, 22–28 (1967).
25. L. Schnieder *et al.*, *Faraday Discuss.* **91**, 259–269 (1991).
26. T. Kinugawa, T. Arikawa, *Jpn. J. Appl. Phys.* **2** (Part 2, No. 4A), L550–L552 (1993).
27. L. Schnieder, W. Meier, K. H. Welge, M. N. R. Ashfold, C. M. Western, *J. Chem. Phys.* **92**, 7027–7037 (1990).
28. Y. Li, G. Wahnström, *Phys. Rev. B* **46**, 14528–14542 (1992).
29. J. Strömquist, L. Bengtsson, M. Persson, B. Hammer, *Surf. Sci.* **397**, 382–394 (1998).
30. A. Hellman *et al.*, *J. Phys. Chem. B* **110**, 17719–17735 (2006).

ACKNOWLEDGMENTS

We thank X. Yang and C. Xiao for helping to set up Rydberg Atom Tagging, R. Bürsing for helping to design the experimental apparatus, and G.-J. Kroes for assisting in the development of the theory. A.M.W. and D.J.A. gratefully acknowledge support from the Humboldt Foundation. We acknowledge support from the Sonderforschungsbereich 1073 under project A04; from the Deutsche Forschungsgemeinschaft (DFG) and the Agence Nationale de la Recherché (ANR) under grant no. WO 1541/1-1; and from the DFG, the Ministerium für Wissenschaft und Kultur (MWK) Niedersachsen, and the Volkswagenstiftung under grant no. INST 186/902-1.

21 September 2015; accepted 30 October 2015
Published online 26 November 2015
10.1126/science.aad4972

GEOPHYSICS

Viscosity jump in Earth's mid-mantle

Maxwell L. Rudolph,[1]* Vedran Lekić,[2] Carolina Lithgow-Bertelloni[3]

The viscosity structure of Earth's deep mantle affects the thermal evolution of Earth, the ascent of mantle plumes, settling of subducted oceanic lithosphere, and the mixing of compositional heterogeneities in the mantle. Based on a reanalysis of the long-wavelength nonhydrostatic geoid, we infer viscous layering of the mantle using a method that allows us to avoid a priori assumptions about its variation with depth. We detect an increase in viscosity at 800- to 1200-kilometers depth, far greater than the depth of the mineral phase transformations that define the mantle transition zone. The viscosity increase is coincident in depth with regions where seismic tomography has imaged slab stagnation, plume deflection, and changes in large-scale structure and offers a simple explanation of these phenomena.

The viscosity of Earth's mantle controls the rate and pattern of mantle convection and, through it, the dynamics of our planet's deep interior, including degassing of and heat transport from the interior, mixing of compositional heterogeneity, plume ascent and passive upwelling, and slab descent. The long-wavelength nonhydrostatic geoid is a key geophysical constraint on Earth's internal viscosity structure. At the largest spatial scales (spherical harmonic degrees 2 to 7), the geoid is most sensitive to density structure and viscosity contrasts in the lower mantle. At smaller scales, the geoid becomes increasingly sensitive to upper mantle structure, which is primarily associated with subducting slabs. Because lateral viscosity variations have minor effects on the geoid at large spatial scales (*1*, *2*)—though they may become more important at shorter length scales (*3*)—it is possible to infer deep mantle viscous layering from geoid observations. However, most studies of Earth's mantle viscosity structure impose layer interfaces to be coincident with seismic velocity discontinuities. Thus, these studies may not resolve viscous layering whose origin is distinct from that of pressure-induced phase changes (e.g., at 410- and 660-km depth), or may miss phase transitions not clearly associated with seismic discontinuities.

We use the long-wavelength nonhydrostatic geoid to infer the mantle radial viscosity structure in a manner distinct from that of previous attempts in three key ways. First, we employ a transdimensional, hierarchical, Bayesian inversion procedure (*4*) that does not specify at the outset the number or location of interfaces in our layered viscosity structure. The Bayesian approach is very attractive for this inverse problem because it yields a posterior probability distribution that can be analyzed to quantify uncertainties of and trade-offs between model parameters (e.g., layer depth and viscosity contrast). Second, we explore various choices for the conversion between seismic velocity anomalies and density anomalies, including depth-dependent conversion factors based on thermodynamic principles, calculated using HeFESTo (*5*). Finally, we use a recent whole-mantle tomographic model, SEMUCB-WM1 (*6*), developed with waveform tomography using highly accurate wave propagation computations, to infer mantle density structure and a modern geoid model based on 10 years of GRACE satellite observations, combined with revised estimates of the hydrostatic flattening of Earth (*7*, *8*).

A posterior probability density function for the radial profile of viscosity is shown in Fig. 1, where the mean (taken in log-space) viscosity at each depth is shown as a purple curve. In this particular inversion, we find evidence for relatively uniform viscosity throughout the upper mantle and transition zone. Below the mantle transition zone, there is a region of lower viscosity and an increase in viscosity between 670- and 1000-km depth. The preferred depth of this viscosity increase can be inferred from Fig. 1B and is centered about 1000 km.

We carried out multiple inversions to explore the effects of (i) our treatment of data and model uncertainty, (ii) the degree of truncation of the spherical harmonic expansion of the geoid used to constrain our models, and (iii) the density scaling $R_{\rho,S} = d \ln \rho / d \ln V_S$ (Fig. 1). We consider features of the viscosity profiles to be robust if they are common among the separate inversions. We find that all solutions place the depth of viscosity increase considerably below 670-km depth, most often near 1000-km depth. This result appears to be independent of assumptions made, including maximum spherical harmonic degree l_{max}, choice of depth-dependent or constant $R_{\rho,S}$, or treatment of data and model covariance (*7*). Other features of the solutions are sensitive to these choices and, therefore, their robustness is proportional to the likelihood of the assumptions from which they result. Inversions with $l_{max} = 7$ (dashed curves in Fig. 2) generally have a more pronounced peak in viscosity in the mid-mantle, underlain by a weaker region between 1500- and 2500-km depth and an increase in viscosity in

[1]Department of Geology, Portland State University, Post Office Box 751, Portland, OR 97207, USA. [2]Department of Geology, University of Maryland, College Park, MD 20742, USA. [3]Department of Earth Sciences, University College London, London WC1E 6BT, UK.
*Corresponding author. E-mail: maxwell.rudolph@pdx.edu

Electron-hole pair excitation determines the mechanism of hydrogen atom adsorption

Oliver Bünermann *et al.*

Science **350**, 1346 (2015);
DOI: 10.1126/science.aad4972